Magnetic study of M-type doped barium hexaferrite nanocrystalline particles.

A. M. Alsmadi[1,2 a)], I. Bsoul[3], S. H. Mahmood[4], G. Alnawashi[1], K. Prokeš[5], K. Siemensmeyer[5], B. Klemke[5], and H. Nakotte[6]

[1]Physics Department, The Hashemite University, 13115 Zarqa, Jordan

[2]Physics Department, Kuwait University, 13060 Safat, Kuwait

[3] Physics Department, Al al-Bayt University, Mafraq, Jordan

[4] Physics Department, The University of Jordan, Amman, Jordan

[5] Helmholtz Zentrum für Matearialien und Energie, 14109 Berlin, Germany

[6] Physics Department, New Mexico State University, Las Cruces, NM 88003, USA

[a)] *Electronic mail: abdel.alsmadi@gmail.com*

Abstract

Co-Ti and Ru-Ti substituted barium ferrite nanocrystalline particles $BaFe_{12-2x}Co_xTi_xO_{19}$ with ($0 \le x \le 1$) and $BaFe_{12-2x}Ru_xTi_xO_{19}$ with ($0 \le x \le 0.6$) were prepared by ball milling method, and their magnetic properties and their temperature dependencies were studied. The zero-field-cooled (ZFC) and field-cooled (FC) processes were recorded at low magnetic fields and the ZFC curves displayed a broad peak at a temperature T_M. In all samples under investigation, a clear irreversibility between the ZFC and FC curves was observed below room temperature, and this irreversibility disappeared above room temperature. These results were discussed within the framework of random particle assembly model and associated with the magnetic domain wall motion. The resistivity data show some kind of a transition from insulator to perfect insulator around T_M. At 2 K, the saturation magnetization slightly decreased and the coercivity dropped dramatically with increasing the Co-Ti concentration x. With Ru-Ti substitution, the

saturation magnetization showed small variations, while the coercivity decreased monotonically, recording a reduction of about 73% at x = 0.6. These results were discussed in light of the single ion anisotropy model and the cationic distributions based on previously reported neutron diffraction data for the CoTi substituted system, and the results of our Mössbauer spectroscopy data for the RuTi substituted system.

Keywords: Ball milling, Barium hexaferrite, ZFC and FC curves, Coercive field, Magnetization, resistivity, dielectric constant.

1. Introduction

M-type barium hexaferrites ($BaFe_{12}O_{19}$) with magnetoplumbite structure have been intensively investigated in the past years as a material for permanent magnets, high-density recording, future multiferroic and high frequency applications [1, 2, 3, 4]. In general, these materials have large saturation magnetization, high coercivity, high Curie temperature, large uniaxial magnetic anisotropy and good chemical stability [5, 6, 7, 8]. Several techniques have been used to prepare M-type hexaferrites such as co-precipitation method [9], sol-gel auto-combustion method [10], hydrothermal process [11], ammonium nitrate melt method [12], microwave-induced combustion [13], mechano-combustion route [14], and ball milling method [15,16]. Ball milling is user-friendly and simple method suitable for the production of powders composed of fine particles smaller than the single domain size. In Barium hexaferrites, the preparation method was found to have significant influence on their magnetic properties.

In order to improve the fundamental magnetic properties of barium hexaferrites, many studies have been concerned with cationic substitutions. Different cations such as

Al [17], Ga, Sc, In [18, 19], and various cationic combination such as, Ni-Ti [20], Co-Zr [21], Co-Sn [22], Zr-Zn [23], Co-Gd [24], Mn-Ti [25], Ni-Ru, Zn-Ru [26], Ti-Ru [27], and Co-Ti [28, 29], were substituted for Fe in Barium hexaferrites. These substitutions were found to cause modifications of the magnetic properties and induce significant changes in several substituted systems.

Co-Ti substituted barium hexaferrites exhibit suitable properties in a wide range of industrial application [28, 29, 30]. It was found that small amounts of Co^{2+} and Ti^{4+} substituting for Fe^{3+} in $BaFe_{12-2x}Co_xTi_xO_{19}$, can substantially reduce the coercive field, H_C, with only a littlie change in saturation magnetization [28, 29, 30, 31, 32, 33, 34]. On the other hand, with Ru-Ti substitution, the saturation magnetization at room temperature was found to increase up to x = 0.2, and then to decrease for higher x values, while the coercivity decreases monotonically, recording a reduction of about 55% at x = 0.4 [27]. These properties, in addition to the large saturation magnetization, good chemical stability, and low switching field distribution make these compounds useful in high density and perpendicular recording. It has, therefore, become important to understand the origin of the property changes when these substitutions are made. Most of the previous investigations on these systems were done at room temperature, where most of the industrial applications take place. However, studying these materials at low temperatures and investigate the dependence of their electrical and magnetic properties on temperature will shed more light onto their magnetic behaviors.

In this contribution, we study the effect of Co-Ti and Ru-Ti substation for Fe on the magnetic properties of barium hexaferrites in $BaFe_{12}O_{19}$ synthesized by ball milling method. The temperature dependence of the magnetic and electrical properties of two barium hexaferrites systems: $BaFe_{12-2x}Co_xTi_xO_{19}$ with $(0 \leq x \leq 1)$ and $BaFe_{12-2x}Ru_xTi_xO_{19}$

with ($0 \le x \le 0.6$) are investigated in a wide range of temperature and magnetic fields in an attempt to understand the magnetic behavior of these hexaferrites.

2. Experimental Procedures

All samples were prepared by ball milling and extracted from the same batch we used in our previous studies [27, 33]. The starting materials for synthesis of $BaFe_{12-2x}Co_xTi_xO_{19}$ with x = 0.0, 0.2, 0.4, 0.6, 0.8, and 1.0 were high purity metallic oxides (Fe_2O_3, TiO and CoO) and barium carbonate ($BaCO_3$). In addition to the above materials, high purity metallic oxide RuO_2 were used for $BaFe_{12-2x}Ru_xTi_xO_{19}$ system and samples were prepared with x = 0.0, 0.1, 0.2, 0.3, 0.4, 0.5, and 0.6. All samples were prepared in a planetary ball-mill (Fritsch Pulverisette-7) with balls and vials of hardened steel. The milling experiment was carried out at 250 rmp for 16 h and the ball to powder ratio was 8:1. The as-milled powders were annealed in air atmosphere at 1100 ºC for 2 h. Further detailed explanation of this treatment is given in references [27, 33]. The phase purity and crystallite sizes in the synthesized samples were checked by x-ray diffraction, and the particle size was determined from the scanning electron microscopy (SEM) imaging.

The magnetization measurements were performed using a Quantum Design superconducting quantum interference device (SQUID). The zero-field-cooled (ZFC) and field-cooled (FC) processes were recorded at low magnetic fields in temperature range from 2 to 300 K. Before each run, samples were demagnetized at 300 K by applying an oscillatory magnetic field, and then cooled down in zero fields to 2 K. At 2 K, a small magnetic field of the order of 100 Oe is applied, and then recording of the magnetization is started as we heat the sample to 300 K. This procedure we denote as the zero-field cooled (ZFC) measurements. At 300 K, the small-applied magnetic field is kept as is and

then samples are cooled again to 2 K, with subsequent recording the magnetization as we heat the sample to 300 K. Such a measurement we denote as a field-cooled (FC) measurements. Some other magnetic and electrical resistivity measurements were carried out using the Quantum Design 14T Physical Properties Measurements System (PPMS).

3. Results and Discussion

3.1 Co-Ti substitutions

X-ray diffractions patterns for $BaFe_{12-2x}Co_xTi_xO_{19}$ are shown in Figure 1. This figure demonstrates that all samples show a hexagonal structure, which matches the standard pattern for hexagonal barium ferrite $BaFe_{12}O_{19}$ with space group $P6_3/mmc$ and lattice parameters a = 5.89 Å and c = 23.20 Å. In addition, small amounts of hematite (less than 5%) were detected in this system. The average crystallite size was calculated using the well-known Scherrer formula, and was found to decrease from about 76 nm for pure sample to 60 nm for the sample with x = 1.0.

Figure 2 shows representative SEM images for the CoTi substituted hexaferrites. The images show relatively narrow particle size distributions for all samples with the average grain size tending to decrease with increasing the substitution level. The average grain size was found to be ~ 330 nm for the pure sample, and ~ 170 nm for the sample with x = 0.8.

Figures 3(a)-3(c) show the ZFC and FC magnetization curves of $BaFe_{12-2x}Co_xTi_xO_{19}$, with x = 0.2, x = 0.8, and x = 1 as a function of temperature measured at 1000 Oe. Similar measurements were done also for the other samples with different concentrations x. For each sample the ZFC magnetization rises from almost the same

value of 4 – 5 emu/g at 2 K to a maximum value at T_M, and then drops exhibiting a broad peak at T_M. Both the maximum magnetization and the temperature at peak value increases with increasing x. The occurrence of the peak can be associated with the magnetic domain wall motion. In zero applied field the magnetic domains are blocked along the corresponding randomly oriented easy directions leading to zero net magnetization in the virgin sample. When the field is switched on at 2K, net magnetization is established in the sample as a consequence of the 180° domain wall flip into the direction of the applied field. However, some domain walls remain pinned due to microstructure in the sample, and can be unpinned by thermal activation [35]. If the field required to unpin the domains (H_{cp}) decreases with increasing temperature as reported for other magnetic systems [36], then as the temperature increases at constant applied field, two effects can occur: First, the usual drop in magnetization due to thermal agitation. Second, the increase in magnetization arising from thermal unpinning of the domain walls and the subsequent domain wall motion induced by the constant magnetizing field at higher temperatures. The competition between these two effects is expected to result in a peak (at T_M), where at temperatures higher than this value, the reduction in magnetization due to thermal effects is dominant, resulting in the observed drop in magnetization. The shift of the peak position to higher temperatures (T_M ~143, 179, and 215 K for x = 0.2, 0.8, and 1 respectively) can be associated with a stronger domain walls pinning as x increases. This is consistent with the observed decrease in crystallite size with increasing x, resulting from the increased level of crystal imperfections which impede the crystal growth on one hand, and increase the domain wall interactions with the crystal imperfections, which are responsible for the wall pinning, on the other hand. The increase in magnetization as x increases is consistent with the reduction in magnetic anisotropy. The observed behavior of magnetization is consistent with the results of previous studies on $BaFe_{12-2x}Ti_xCo_x$ with x = 0.8 [11, 37,

38]. In these investigations the occurrence of the peak was attributed to ferromagnetic-superparamagnetic transition in the nano-sized particles. However, in a recent study [39] it was shown that such transition occurs near the Curie temperature of the hexaferrite which was ~ 700 K for the Ga substituted hexaferrites, resulting in a large Hopkinson peak just below T_C. At lower temperatures the particle moments are blocked and no superparamagnetic behavior is anticipated.

Figures 3(a)-3(c) also show a clear irreversibility between the ZFC and FC measurements. The FC magnetization is always above the ZFC up to temperatures even above room temperature for lower Co-Ti concentrations and up to about room temperature for x = 0.8. This could be attributed to easier unpinning of the domain walls by the constant field at higher temperatures. For all different concentrations, the FC magnetization reaches almost a constant value below a given temperature T^*, below which the domain wall motion is saturated and no further increase in magnetization occurs at lower temperatures. The small drop in magnetization below T* for the sample with x = 1.0 is associated with different distributions of pinning fields resulting in the double peak structure for this sample, where a second peak seems to occur around 130 K. This could also indicate a presence of some degree of reversibility in domain wall pinning in this sample at low temperatures.

Figure 4(a) shows magnetization hysteresis curves of the $BaFe_{12-2x}Co_xTi_xO_{19}$ series for x = 0.0, 0.4 and 0.8, measured at 2 K. Similar measurements were done using the other samples with different concentrations, both at 2 K and at room temperature. The coercive field strength for the non-substituted sample is about 3.2 kOe. This value is in good agreement with the reported value for a similar sample grown by ball milling method [15] but smaller than the reported values for similar samples grown by different

techniques [12, 30, 40]. The saturation magnetization at 2 K is obtained from the law of approach to saturation [41]:

$$M = M_s(1 - A/H - B/H^2) + \chi H \qquad (1)$$

where M_s is the spontaneous magnetization of the domains, χH term is associated with the field-induced increase in the spontaneous magnetization of the domains, the material constant A arises from sample inhomogeneities, and B represents the magnetocrystalline anisotropy contribution. The magnetization data in the field range between about 8 kOe and 12 kOe were plotted against $1/H^2$, and straight lines were obtained indicating that in this range the both A and the last term in equation (1) are negligible. The intercepts of the straight lines gave the saturation magnetizations for the samples. The slopes of the lines were used to determine the anisotropy field from the relation:

$$B = H_a^2/15 \qquad (2)$$

The first anisotropy constant is then evaluated using the relation [41]:

$$H_a = 2K_1/M_s \qquad (3)$$

The saturation magnetization obtained from the linear fit, and the coercivity determined from the hysteresis loops are shown in Fig. 2(b). The saturation magnetization and the coercivity exhibits a behavior similar to that reported at room temperature [33]. The saturation magnetization at 2 K ranges from 93 emu/g for the non-substituted sample to 77.4 emu/g for the sample with x = 1.0. The value for the non-substituted sample at 5 K is only 7% smaller than the theoretically predicted value at zero temperature corresponding to a net magnetic moment of 20 μ_B per formula unit [41]. This reduction could be partially associated with the small amount of hematite observed by XRD. The

reduction in saturation magnetization for x = 1.0 down to about 83% of the value for the non-substituted sample is associated with preferential site occupation of Co^{2+} and Ti^{4+} ions at spin-up and spin-down sites. The value of M_s = 77.4 emu/g corresponds to a net magnetic moment of 16.6 μ_B at T = 0.

In the hexaferrite lattice there are three spin-up (2a, 2b and 12k) magnetic sites occupied by 8 metallic ions per formula, and two spin-down ($4f_1$, $4f_2$) sites occupied by 4 ions. Previously reported results based on careful analysis of the neutron diffraction and Mössbauer data indicated that Co^{2+} ions preferred tetrahedral $4f_1$ spin-down sites, where Ti^{4+} ions distribute themselves at both spin-up (12*k*, 2*a*) sites as well as at spin-down $4f_2$ site [42, 43]. Based on this cationic preferential site occupation, and assuming a magnetic moment of 3 μ_B per Co^{2+} ion in the tetrahedral site, 5 μ_B per Fe^{3+} ion, and 0 μ_B per Ti^{4+} ion, the fraction (denoted as z) of Ti^{4+} ions at spin-up sites can be calculated from the observed magnetic moment per formula (μ) as follows:

$$\mu = 5\,\mu_B.\,[8 - z] - 3\,\mu_B.[x] - 5\,\mu_B.\,[4 - x - (x - z)] = (20 + 7x - 10z)\,\mu_B \qquad (4)$$

Formatted: English (U.S.)

Formatted: English (U.S.)

Based on this equation and the magnetic moments per formula unit for the substituted hexaferrites the z fraction was calculated and the results are summarized in Table 1.

Table 1: Magnetic moment (in μ_B per formula) and the z fraction of Ti^{4+} ions at spin-up sites.

x	μ	z
0.2	19.4	0.20
0.4	19.2	0.36
0.6	18.8	0.54
0.8	18.0	0.76
1.0	16.6	1.04

It is evident that the fraction of Ti^{4+} ions in the spin-up sublattices is nearly equal to the value of x, indicating that Ti^{4+} ions in our samples occupy spin-up sites, with no preference for spin-down sites.

While the saturation magnetization, M_S, slightly decreased with Co-Ti substitutions, the coercivity, H_C, dropped dramatically from about 3.2 kOe to 1.02 kOe as x increases from 0.0 to 1.0. This indicates that this system has potential for magnetic recording applications since one can easily control H_C to meet the requirements of different magnetic recording systems, while still maintaining a relatively high value of M_S. The behavior of the coercivity is consistent with the general behavior of the anisotropy field and saturation magnetization shown in Fig. 4(c). Fig. 4(c) also shows the variation of the first anisotropy constant with x. The fast drop in H_a and K_1 for x > 0.4 could be associated with the onset of a transition from uniaxial anisotropy to planar anisotropy as a consequence of the increased level of Co^{2+} ions in the lattice.

3.2 Ru-Ti substitutions

X-ray diffraction patterns (Figure 5) for the RuTi substituted hexaferrites indicated the presence of a single hexaferrite phase consistent with the standard pattern JCPDS: 043-0002. The variation in lattice parameters was less than 0.2%, and the cell volume was found to be almost constant (0.698 nm^3) for all samples. The X-ray density for the samples was then evaluated and found to range from 5.3 g/cm^3 to 5.41 g/cm^3 as x changes from 0.0 to 0.6. The average crystallite size was calculated and found to change from 69 nm for x = 0.1 to 77 nm for x = 0.4.

Transmission electron microscopy (TEM) images obtained for all samples indicated that the average grain sizes of all RuTi substituted hexaferrite were larger than

that for the un-substituted sample. Figure 6 shows the images for the representative samples with x = 0.0 and 0.4. The average particle size increases from about 45 nm for pure sample up to about 180 nm with increasing substitution. These small particle sizes indicate that all samples above room temperature consist of single magnetic domain particles with sizes smaller than the critical single domain size of 460 nm [44].

Figure 7 shows room temperature Mössbauer spectra for the samples with x up to 0.4. Each spectrum consists of five magnetic sextets corresponding to the five crystallographic sites of the hexaferrite lattice. This indicates that all hexaferrites are magnetically ordered at room temperature. The spectra were fitted with four sextets due to the similarity of the hyperfine parameters of the 2a and $4f_1$ components. The sub-spectral intensities were found to fluctuate by 1 – 2% with increasing x, which is within the experimental uncertainty. Thus the intensities could not give a clear picture of the site preference of the various cations. As a consequence, we used the variations in the hyperfine parameters to make a conclusion regarding the cationic distributions over the sites. Our results indicated that the Ti^{2+} ions prefer $4f_2$ and/or 2a sites, while Ru^{4+} ions prefer $4f_1$ sites up to x = 0.2, and then starts to partially substitute Fe^{3+} ions at 2b sites for higher Ru concentrations [26, 27].

Figures 8(a)-8(c) show the ZFC and FC magnetization curves of $BaFe_{12-2x}Ru_xTi_xO_{19}$, with x = 0.0, 0.3, and x = 0.6 as a function of temperature measured at small magnetic field of 100 Oe. We observed similar magnetization behavior even in a smaller magnetic field of 40 Oe. The data show a clear irreversibility between the ZFC and FC measurements, even at room temperature for higher Ru-Ti concentrations. The ZFC curves show wide maxima at T_M ~ 29, 80, 62, 50 and 57 K for x = 0.1, 0.2, 0.3, 0.4 and

0.6, respectively. Clearly, no systematic changes were observed in the value of T_M as a function of the Ru-Ti concentrations. This can be understood by considering that the TEM images for the samples indicated that while the average particle size of the non-substituted samples is about 45 nm, the substituted samples contain much larger particles. However, the crystallinity improves slightly with the increased level of substitution. This explains the absence of a peak in the ZFC curves for the x = 0 sample, which consist of small single domain particles. The peaks in the ZFC curves for the substituted samples are consistent with the presence of multidomain particles at low temperatures with similar sources of pinning mechanisms.

In order to get more information on the nature of the transition at T_M, we extended our study to electrical resistivity measurements using the Quantum Design 14T Physical Properties Measurements System (PPMS). We started to measure the electrical resistivity with the standard four-point AC method. However, for temperatures below 270 K, the samples show a very high resistance, which is above the resistance bridge limits. In this temperature range, the resistivity was measured using the capacitive (conductivity) method. For this method, the sample was prepared as a small disc (diameter of 2mm, and a thickness of 0.8 mm) and then inserted between the plates of a capacitor. Simultaneous measurements of both the capacitance and the loss tangent in the circuit were recorded as a function of temperature at constant frequency of 1000Hz. From the capacitance data, the dielectric constant was determined. On the other hand, the loss in the circuit is directly proportional to the resistance of the sample. The electrical resistivity measurements taken from this method were then normalized to the resistivity values taken with the standard four-point AC method. In Figure 9, the temperature dependence of the electrical resistivity $BaFe_{12-2x}Ru_xTi_xO_{19}$ with x = 0.5, measured at various magnetic fields is shown. Similar behavior was observed in other

samples with different Ru-Ti and Co-Ti concentrations. The resistivity data show some kind of a transition from insulator to perfect insulator below T_M . No significant magnetic filed effects were observed on the resistivity behavior even in field of 4 T. While this observation indicates that there are no magnetoresistance effects in the system under investigation, the resistivity behavior could be associated with a perfectly insulating ferroelectric state below about 40 K, which is destroyed as the conductivity rises above this temperature.

Figure 10(a) shows the magnetization hysteresis curves of the $BaFe_{12-2x}Ru_xTi_xO_{19}$ for x = 0.0, 0.1, 0.3 and 0.6, measured at 5 K. Similar measurements were done also for the other samples with different Ru-Ti substitutions, both at 5 K and at room temperature. The magnetization curves for the non-substituted sample belong to hard magnetic materials with coercive field strength of 3.750 kOe at 5K. This value is slightly lower than that of 4.0 kOe observed at room temperature, which is a further indication of the multidomain structure at low temperatures. The saturation magnetization at 5 K obtained from the linear fit of eq. (1), and the coercivity determined from the hysteresis loops are shown in Fig. 10(b). This figure demonstrates that the saturation magnetization exhibits a behavior similar to that reported at room temperature [27], with saturation magnetization ranging from 88.0 emu/g to 81.3 emu/g. The coercivity, H_C, drops dramatically from about 3.75 kOe to 0.7 kOe as x increases from 0.0 to 0.6. The increase in saturation magnetization in the range of x between 0.0 and 0.2 is a consequence of the substitution of Ti^{2+} and Ru^{4+} ions at $4f_2$ and $4f_1$ spin-down sites, respectively, as indicated by the results of Mössbauer spectroscopy. However, the decrease in saturation magnetization at higher concentrations is associated with the progressive substitution at 2a and 2b spin-up sites. The behavior of the coercivity is consistent with the general behavior of the anisotropy field and saturation magnetization

shown in Fig. 10(c). The initial large drop in coercivity in the concentration region between 0.0 and 0.2 is associated with the decrease in anisotropy field and increase in saturation magnetization according to the relation:

$$H_c = C(H_a - N_d M_s) \qquad (5)$$

where *C* is a constant which depends on the nature and degree of alignment of the magnetic particles, and N_d is the demagnetization factor which depends on the shape of the particles. For x > 0.2, the decrease in saturation magnetization reduces the rate of the drop in coercivity.

Fig. 10(c) also shows the variation of the first anisotropy constant with x. The value of 3.33 x 10^6 erg/cm^3 is in excellent agreement with the reported value for pure BaM hexaferrite [41].

Figure 11 shows the isothermal magnetization hysteresis curves of the $BaFe_{12-2x}Ru_xTi_xO_{19}$ with x = 0.1, measured at several temperatures. The saturation magnetization decreases from 94.6 emu/g at 5 K to 50.8 emu/g at 400 K. On the other hand, the coercivity, H_C, increases from 1.75 kOe at 5 K to 4.5 kOe at 400 K. The appreciable increase in coercivity at 400 K is a consequence of the thermally assisted domain wall de-pinning and the transition to single domain particles at temperatures above T_M.

4. Conclusion

In conclusion, Co-Ti and Ru-Ti substituted barium ferrite nanocrystalline particles: $BaFe_{12-2x}Co_xTi_xO_{19}$ with $(0 \le x \le 1)$ and $BaFe_{12-2x}Ru_xTi_xO_{19}$ with $(0 \le x \le 0.6)$

have been prepared by ball milling method. The static magnetic properties of the powders and their temperature dependencies were studied. The ZFC and FC curves of all samples below room temperature display behavior consistent with the thermally aided unpinning of domain walls and the subsequent domain wall motion. The position of the observed peak in ZFC curves at a temperature T_M seems to be sensitive to the microstructure of the prepared samples. We also observed a clear irreversibility between the ZFC and FC curves, which disappears as we approach the room temperature region. The resistivity data show some kind of a transition from insulator to perfect insulator below T_M . This is associated with a transition to a ferroelectric state below T_M. T_M shifts to higher values by increasing the Co-Ti concentration x due to the increased level of crystal imperfections, while no systematic changes were observed in T_M with Ru-Ti concentrations due to similarity of the microstructure in the samples of this system. At 2 K, doping barium ferrite particles with Co-Ti results in a significant decrease in their magnetic coercivity with a small decrease of their saturation magnetization. In addition, doping barium ferrite with Ru-Ti results in small variations in their saturation magnetization and a significant drop in their coercivity, recording a reduction of about 73% at x = 0.6.

Acknowledgements

We would like to thank the Deutsche Forscungsgemeinschaft German Research Foundation (DFG) for providing Dr. A. M. Alsmadi with a supported fellowship to stay at the Helmholtz-Zentrum Berlin for 3 months during this project.

References

[1] R.C. Pullar, Prog. Mater. Sci. **57**, 1191 (2012)

[2] U. Özgür, Y. Alivov, and H.J. Morkoç. Mater. Sci.: Mater. Electron **20**, 789 (2009)

[3] T. Kimura, Annu. Rev. Condens. Matter Phys. **3**, 93 (2012)

[4] G. Tan and X. Chen, J. Magn. Magn. Mater. **327**, 87 (2013)

[5] Y.Y. Meng, M.H. He, Q. Zeng, D.L. Jiao, S. Shukla, R.V. Ramanujan, and Z.W. Liu, J. Alloys Comp. **583**, 220 (2014)

[6] J. Kreisel, H. Vincent, F. Tasset, and P. Wolfers, J. Magn. Magn. Mater. **213**, 262 (2000)

[7] G. Li, G. Hu, H. Zhou, X. Fan, and X. Li, Mater. Chem. Phys. **75**, 101 (2002)

[8] G-H. An, T-Y. Hwang, J. Kim, JB. Kim, N. Kang, S. Kim, Y-m. Choi, and Y-H. Choa, J. Alloys Comp. **583**, 145 (2014)

[9] K. S. Moghaddam, and A. Ataie, J. Alloys Comp. **426**, 415 (2006)

[10] I. Ali, M.U. Islam, M.S. Awan, and M. Ahmad, J. Alloys Comp. **547**, 118 (2013)

[11] M. Drofenik, I. Ban, D. Makovec, A. Žnidaršič, Z. Jagličić, D. Hanžel, and D. Lisjak, Mater. Chem. Phys. **127**, 415 (2011)

Formatted: English (U.S.)

Formatted: German (Germany)

[12] U. Topal, H. Ozkan, and L. Dorosinskii, J. Alloys Comp. **428**, 17 (2007)

[13] Y. P. Fu, C. H. Lin, and K. Y. Pan, J. Appl. Phys. **42**, 2681 (2003)

[14] A. Ataie and S. E. Zojaji, J. Alloys Comp. **431**, 331 (2007)

[15] V. Babu and P. Padaikathan, J. Magn. Magn. Mater. **241**, 85 (2002)

[16] I. Bsoul, S.H. Mahmood, A-F. Lelooh, and A. Al-Jamel, J. Alloys Comp. **551**, 490 (2013)

[17] S. Wang, J. Ding, Y. Shi, and Y. J. Chen, J. Magn. Magn. Mater. **219**, 206 (2001)

[18] T. M. Clark, B. J. Evans, and G. K. Thomson, J. Appl. Phys. **85**(8), 5229 (1999)

[19] I. Bsoul and S. H. Mahmood, J. Alloys Comp. **489**, 110 (2010)

[20] X. Tang, Y. Yang, and K. Hu, J. Alloys Comp. **477**, 322 (2009)

[21] Ch. Venkateshwarlu, Ch. Ashok, B. A. Rao, D. Ravinder, and B. S. Boyanov, J. Alloys Comp. **426**, 1 (2006)

[22] X. Gao, Y. Du, X. Liu, P. Xu, and X. Han, Mater. Res. Bull. **46**, 643 (2011)

[23] M. J. Iqbal, M. N. Ashiq, and P. H. Gomez, J. Alloys Comp. **478**, 736 (2009)

Formatted: German (Germany)

Formatted: German (Germany)

[24] G. Litsardakis, I. Manolakis, and K. Efthimiadis, J. Alloys Comp. **427**, 194 (2007)

[25] F. Tabatabaie, M. H. Fathi, A. Saatchi, and A. Ghasemi, J. Alloys Comp. **470**, 332 (2009)

[26] A. González-Angeles, G. Mendoza-Suárez, A. Grusková, J. Lipka, M. Papánová and J. Sláma, J. Magn. Magn. Mater. **285**, 450 (2005)

[27] I. Bsoul, S. H. Mahmood, and Abdel-Fatah Lehlooh, J. Alloys Comp. **498**, 157 (2010)

[28] W. Zhang, Y. Bai, X. Han, L. Wang, X. Lu, and L. Qiao, J. Alloys Comp. **546**, 234 (2013)

[29] F. Tabatabaie, M. H. Fathi, A. Saatchi, and A. Ghasemi, J. Alloys Comp. **474**, 206 (2009)

[30] S. Y. An, I. B. Shim, and C. S. Kim, J. Appl. Phys. **91**, 8465 (2002)

[31] N. Koga and T. Tsutaoka, J. Magn. Magn. Mater. **313**, 168 (2007)

[32] G. B. Teh, N. Saravanan, and D. A. Jefferson, Mater. Chem. Phys. **105**, 253 (2007)

[33] I. Bsoul, Jordan J. Phys. **2**, 95 (2009)

[34] T. Tsutaoka and N. Koga, J. Magn. Magn. Mater. **325**, 36 (2013)

[35] P. Gaunt, IEEE Tans. Magn. **5**, 2030 (1983)

[36] G. Vértesy, I. Tomaáš, and Z. Vértesy, J. Phys. D: Appl. Phys. **35**, 625 (2002)

[37] X. Batlle, M. Garcìa del Muro, J. Tejada, H. Pfeiffer, P. Görmert and E. Sinn, IEEE Transactions on Magnetics **30**, 708 (1994)

[38] X. Batlle, M. Garcìa del Muro, J. Tejada, H. Pfeiffer, P. Görmert and E. Sinn, J. Appl. Phys. **74** , 3333 (1993)

[39] S.H. Mahmood and I. Bsoul, EPJ Web of Conferences **29**, 00039 (2012)

[40] H. Shang, J. Wang, and Q. Liu, Mater. Sci. Eng. A **456**, 130 (2007)

[41] B. D. Cullity and C. D. Graham, Introduction to Magnetic Materials, 2nd ed. Wiley, Hoboken, New Jersy, 2009

[42] P. Wartewig, M.K. Krause, P. Esquinazi, S. Rösler, and R. Sonntag, J. Magn. Magn. Mater. **192**, 83 (1999)

[43] X. Batlle, X. Obradors, J. Rodriguez-Carvajal, M. Pernet, M.V. Cabañas, and M. Vallet, J. Appl. Phys. **70**, 1614 (1991)

Formatted: German (Germany)

Formatted: German (Germany)

Formatted: German (Germany)

[44] L. Rezlescu, E. Reslescu, and P. D. Papo, J. Magn. Magn. Mater. **193**, 288 (1999)

FIGURES CAPTIONS

Figure 1. X-ray diffraction patterns for $BaFe_{12-2x}Co_xTi_xO_{19}$ hexaferrites.

Figure 2. SEM images for representative samples of $BaFe_{12-2x}Co_xTi_xO_{19}$ hexaferrites with a) x = 0.0, b) x = 0.4, and c) x = 0.8.

Figure 3. (Color online) Zero-field-cooled and field-cooled magnetizations of $BaFe_{12-2x}Co_xTi_xO_{19}$ as a function of temperature measured at 1000 Oe for a) x = 0.2, b) x = 0.8, and c) x = 1.

Figure 4. (Color online) (a) SQUID Magnetization loops of the $BaFe_{12-2x}Co_xTi_xO_{19}$ samples with x = 0.0, 0.4 and 0.8 as a function of the applied magnetic field measured at 2 K. (b) Saturation magnetization and coercivity of $BaFe_{12-2x}Co_xTi_xO_{19}$ as a function of Co-Ti concentration (x). (c) Anisotropy field and the first anisotropy constant of $BaFe_{12-2x}Ru_xTi_xO_{19}$ as a function of Co-Ti concentration (x).

Figure 5. X-ray diffraction patterns for $BaFe_{12-2x}Ru_xTi_xO_{19}$ hexaferrites.

Figure 6. TEM images for representative samples of $BaFe_{12-2x}Ru_xTi_xO_{19}$ hexaferrites with a) x = 0.0 and b) x = 0.4.

Figure 7. (Color online) Room temperature Mössbauer spectra for $BaFe_{12-2x}Ru_xTi_xO_{19}$ hexaferrites.

Figure 8. (Color online) Zero-field-cooled and field-cooled magnetizations of $BaFe_{12-2x}Ru_xTi_xO_{19}$ as a function of temperature measured at 100 Oe for a) x = 0.0, b) x = 0.3, and c) x = 0.6.

Figure 9. (Color online) Electrical resistivity of the $BaFe_{12-2x}Co_xTi_xO_{19}$ sample with x = 0.5 as a function of temperature measured at different applied magnetic fields.

Figure 10. (Color online) (a) SQUID Magnetization loops of the $BaFe_{12-2x}Ru_xTi_xO_{19}$ samples with x = 0.0, 0.1, 0.3 and 0.6 as a function of the applied magnetic field measured at 5 K. (b) Saturation magnetization and coercivity of $BaFe_{12-2x}Ru_xTi_xO_{19}$ as a function of Ru-Ti concentration (x). (c) Anisotropy field and the first anisotropy constant of $BaFe_{12-2x}Ru_xTi_xO_{19}$ as a function of Ru-Ti concentration (x).

Figure 11. (Color online) SQUID magnetization loops of the $BaFe_{12-2x}Co_xTi_xO_{19}$ sample with x = 0.1 as a function of the applied magnetic field measured at different temperatures.

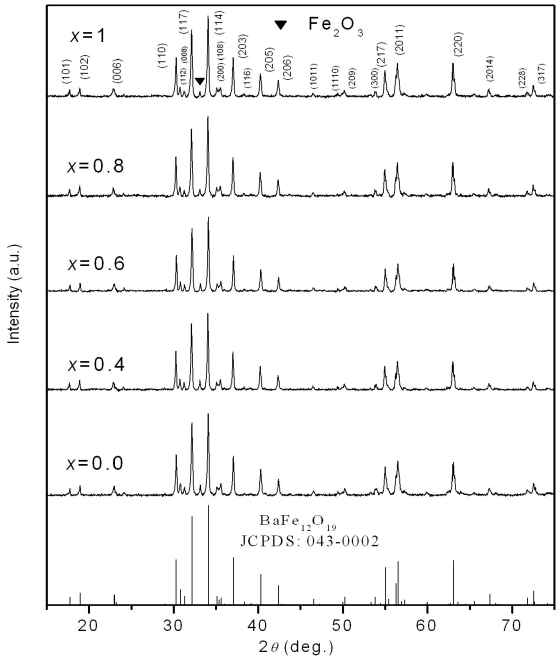
x=1
Fe2O3
(101)
(102)
(006)
(110)
(117)
(012)
(008)
(300)(1 0 8)
(114)
(203)
(116)
(205)
(206)
(1011)
(1110)
(209)
(300)
(217)
(2011)
(220)
(2014)
(228)
(317)
x=0.8
x=0.6
x=0.4
x=0.0
BaFe12O19
JCPDS: 043-0002
Intensity (a.u.)
20
30
40
50
60
70
2θ (deg.)

FIGURE 1

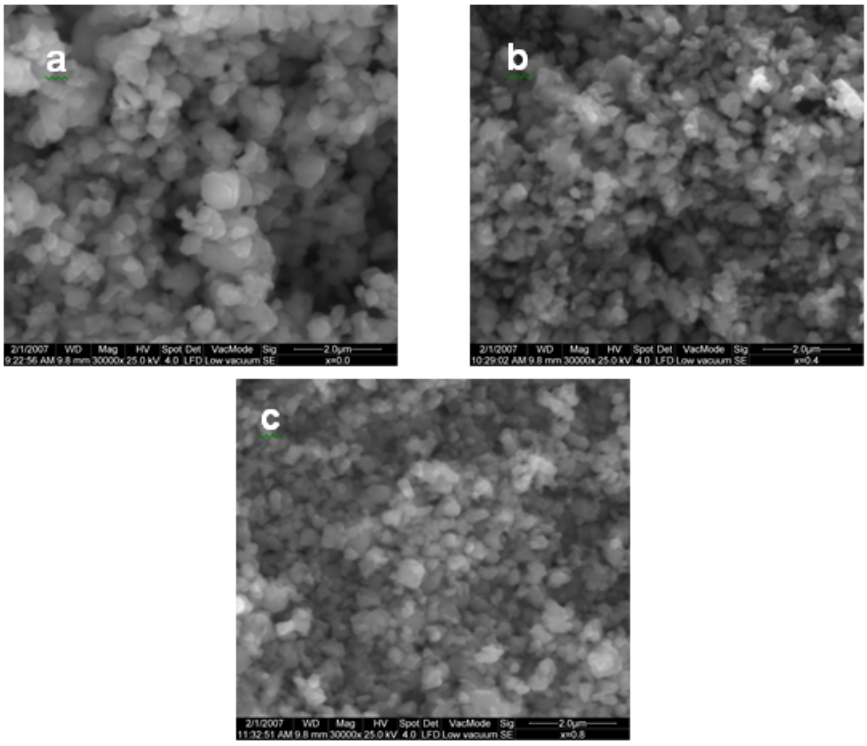

FIGURE 2

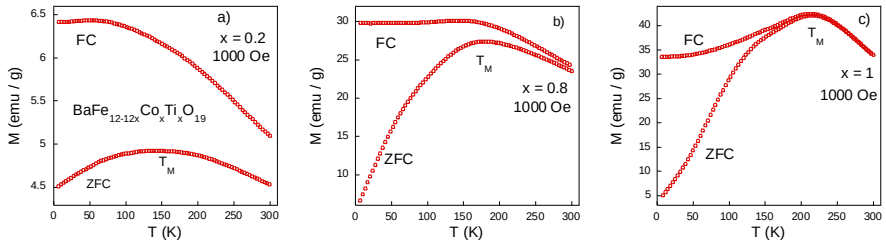
a)
x = 0.2
1000 Oe
FC
BaFe12-12xCoxTixO19
TM
ZFC
M (emu / g)
T (K)
b)
FC
TM
x = 0.8
1000 Oe
ZFC
M (emu / g)
T (K)
c)
FC
TM
x = 1
1000 Oe
ZFC
M (emu / g)
T (K)

FIGURE 3

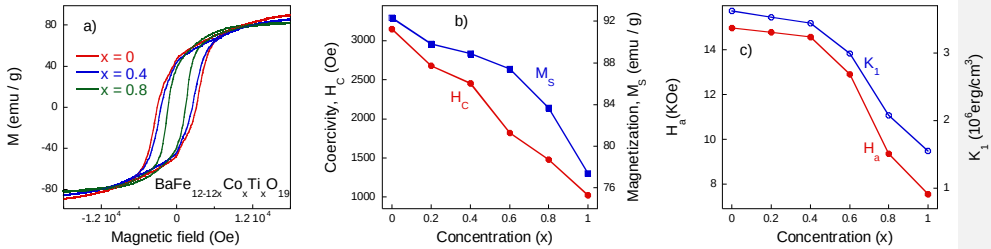
a)
x = 0
x = 0.4
x = 0.8
BaFe12-2xCoxTixO19
M (emu / g)
Magnetic field (Oe)
b)
Coercivity, HC (Oe)
Magnetization, MS (emu / g)
HC
MS
Concentration (x)
c)
Ha (KOe)
K1 (10^6erg/cm^3)
Ha
K1
Concentration (x)

FIGURE 4

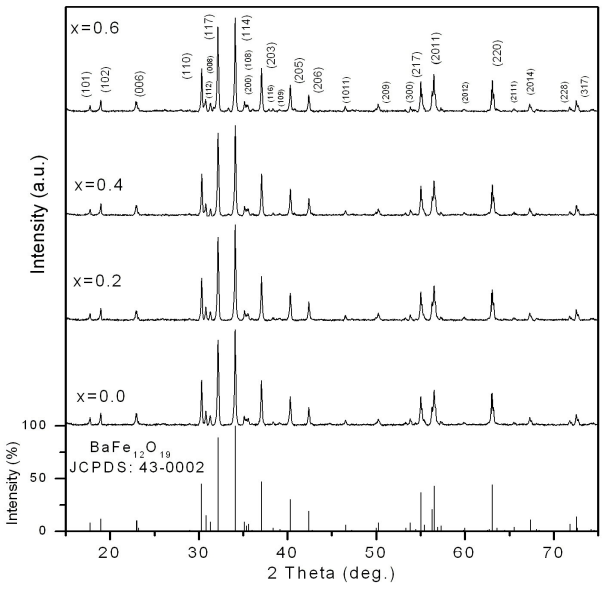
x=0.6
(101)
(102)
(006)
(110)
(107)
(116)
(109)
(205)
(206)
(1011)
(209)
(300)
(217)
(2011)
(2012)
(220)
(2111)
(2014)
(228)
(317)
x=0.4
x=0.2
x=0.0
Intensity (a.u.)
BaFe12O19
JCPDS: 43-0002
Intensity (%)
100
50
0
20
30
40
50
60
70
2 Theta (deg.)

FIGURE 5

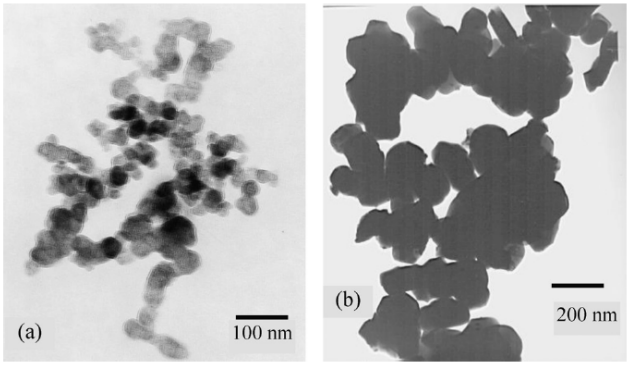

FIGURE 6

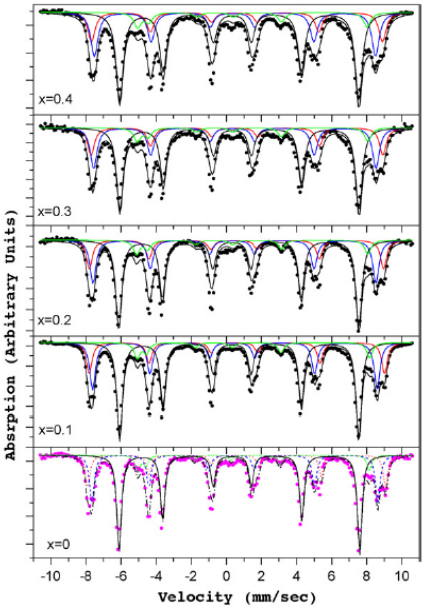
x=0.4
x=0.3
x=0.2
x=0.1
x=0
Absrption (Arbitrary Units)
-10
-8
-6
-4
-2
0
2
4
6
8
10
Velocity (mm/sec)

Figure 7

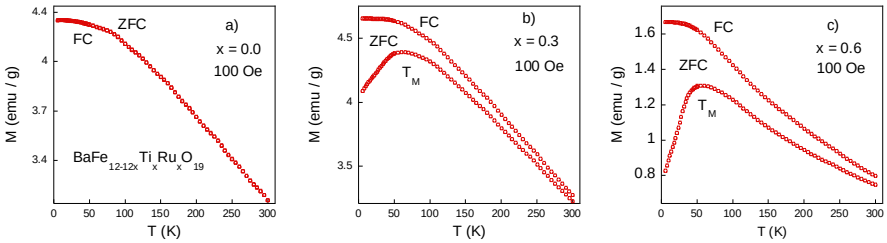
a)
x = 0.0
100 Oe
ZFC
FC
BaFe12-12x Tix Rux O19
M (emu / g)
T (K)
b)
x = 0.3
100 Oe
FC
ZFC
TM
M (emu / g)
T (K)
c)
x = 0.6
100 Oe
FC
ZFC
TM
M (emu / g)
T (K)

FIGURE 8

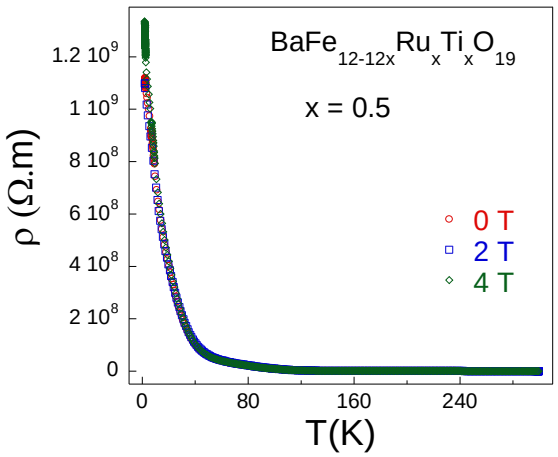
BaFe12-12xRuxTixO19
x = 0.5
0 T
2 T
4 T
ρ (Ω.m)
T(K)
1.2 10^9
1 10^9
8 10^8
6 10^8
4 10^8
2 10^8
0
0
80
160
240

FIGURE 9

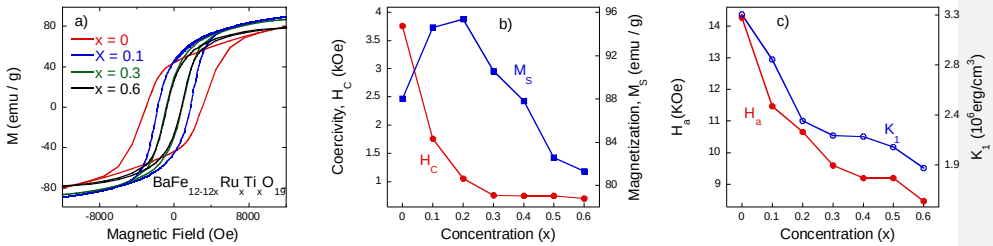
a)
x = 0
X = 0.1
x = 0.3
x = 0.6
M (emu / g)
Magnetic Field (Oe)
BaFe12-2xRuxTixO19
b)
Coercivity, HC (kOe)
Magnetization, MS (emu / g)
HC
MS
Concentration (x)
c)
Ha (KOe)
K1 (10^6 erg/cm^3)
Ha
K1
Concentration (x)

FIGURE 10

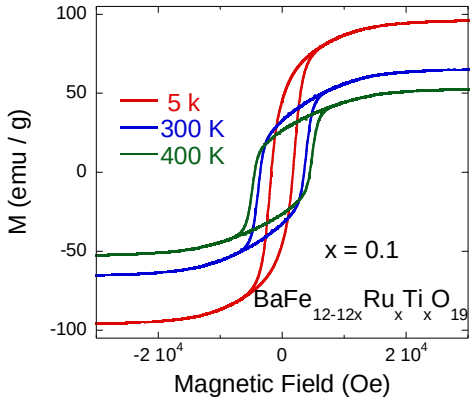
100
50
0
-50
-100
M (emu / g)
5 k
300 K
400 K
x = 0.1
BaFe12-12x Rux Tix O19
-2 10^4
0
2 10^4
Magnetic Field (Oe)

FIGURE 11